ACS APPLIED MATERIALS & INTERFACES

Research Article

www.acsami.org

Atomic-Scale Characterization of Oxide Thin Films Gated by Ionic Liquid

Andrew C. Lang,[†] Jennifer D. Sloppy,[†] Hessam Ghassemi,[†] Robert C. Devlin,[†] Rebecca J. Sichel-Tissot,[†] Juan-Carlos Idrobo,[‡] Steven J. May,[†] and Mitra L. Taheri*[,†]

[†]Department of Materials Science and Engineering, Drexel University, Philadelphia, Pennsylvania 19104, United States

[‡]Center for Nanophase Materials Sciences, Oak Ridge National Laboratory, Oak Ridge, Tennessee 37831, United States

ABSTRACT: Ionic liquids (ILs) have received considerable interest for use in electrostatic gating in complex oxide systems. Understanding the ionic liquid/oxide interface, and any bias-induced electrochemical degradation, is critical for the interpretation of transport phenomena. The integrity of the interface between ionic liquid 1-ethyl-3-methylimidazolium hexafluorophosphate and $La_{1/3}Sr_{2/3}FeO_3$ under various biasing conditions was examined by analytical transmission electron microscopy, and we report film degradation in the form of an irreversible chemical reaction regardless of the applied bias. This results in an intermixing region of 4−6 nm at the IL/oxide interface. Electron energy loss spectroscopy shows La and Fe migration into the ionic liquid, resulting in secondary phase formation under negative bias. Our approach can be extended to other ionic liquid/oxide systems in order to better understand the electrochemical stability window of these device structures.

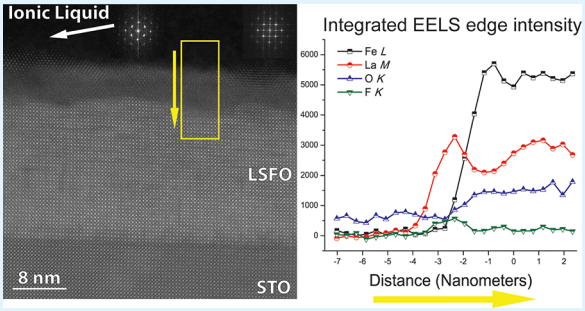

KEYWORDS: *$La_{1/3}Sr_{2/3}FeO_3$, ionic liquid gating, transmission electron microscopy, charge accumulation, electron energy loss spectroscopy, oxide thin film*

INTRODUCTION

Materials that experience electronic phase transitions, such as metal−insulator transitions or semiconducting−superconducting transitions, are excellent candidates for electronic devices like field-effect transistors.[1−4] Such devices require that switching between conductive and insulating states be achieved by an applied bias.[2,5] The use of conventional dielectrics for electrostatic carrier doping and the limitations imposed by dielectric breakdown are often an impeding factor in field-effect-based control of metal−insulator phase transitions.[1,6]

Ionic liquids (ILs) have been shown to be an innovative means of inducing and maintaining charge accumulation, that can be orders of magnitude larger than that achieved with solid dielectrics.[7−13] ILs are binary salts that are chemically and thermally stable when heated above their melting temperatures; they are highly polar, have low-melting temperatures, and do not require solvents.[7] Charge accumulation occurs via an applied bias to the IL, which separates ions within the IL and forms an electric-double-layer (EDL) on the ends of the electrodes. The EDL is a densely packed layer of ions, separated from the channel material by approximately 1 nm, which generates extremely high capacitance (up to 10 μF^9) and can induce a sheet carrier density on the order of 10^{14} cm^{-2} within the adjacent channel material.[10,12] These properties have fueled much research related to the use of ILs as liquid gate dielectrics;[11,14−19] however, recent research has revealed some limitations of using ILs as a biasing medium due various electrochemical effects.[6,10,12,15,20−22] In the case of $NdNiO_3$, while reversible charge accumulation was achieved at biases between 0 and −2.5 V, a large irreversible change in electronic transport behavior was observed when $NdNiO_3$ thin films were gated with $V_G < -2.5$ V, which indicated operation outside of a safe electrochemical window.[12] In $SrTiO_3$ EDL-transistors, it was found that electrochemical reactions dominate the change in electronic transport behavior observed when IL is biased greater than 3.75 V and that changes in oxygen stoichiometry may be at fault.[6,10,20] Additionally, the electrical changes induced by IL-gating of VO_2 EDL-transistors has also been attributed to electrochemical effects.[21,23] Typically, it is postulated that there exists a distinct energy barrier above which an applied bias will cause an irreversible electrochemical reaction between an IL and an oxide thin film. Presumably, the voltage threshold for electrochemical reactions depends on the compositional and structural specifics of the ionic liquid and oxide materials investigated; as such, accessible techniques that probe the integrity of the oxide film, at the atomic scale, during ionic liquid gating can provide tremendous benefit in elucidating the role of electrostatics and electrochemistry in field-effect induced electronic transport behavior.

To date, several studies have employed atomic force microscopy as a means to probe the IL/solid interface.[24−26] While they have successfully imaged IL/solid interfaces and

Received: July 16, 2014
Accepted: September 3, 2014
Published: September 4, 2014

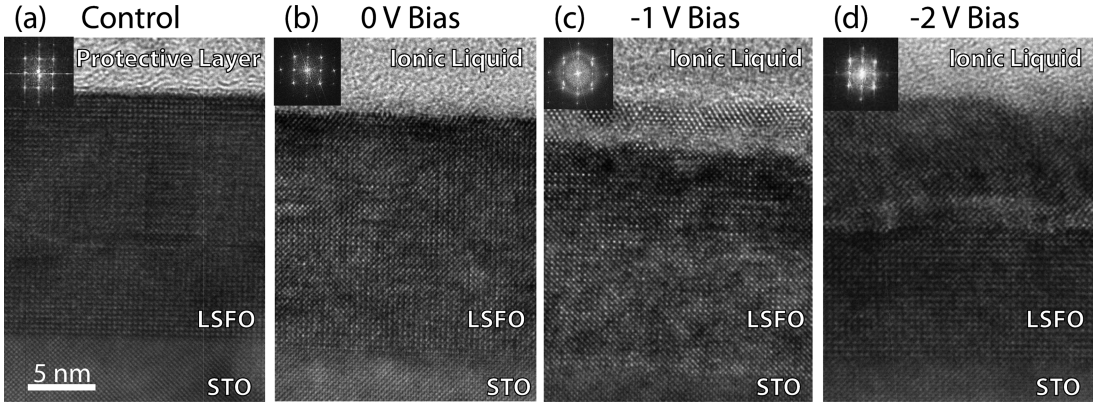

Figure 1. TEM images of the IL/LSFO interface with inset power spectra from across the LSFO film: (a) Control LSFO thin film sample with no IL and no bias. (b) 0 V sample showing a decrease in LSFO film thickness and uneven IL/LSFO interface. (c) −1 V sample showing a secondary phase on top of the LSFO film. (d) −2 V sample showing degradation of the entire top half of the LSFO film. The scale bar is consistent across all four images, and the electron beam is normal to the (001).

revealed the local arrangement of IL molecules, their findings are hindered by the high viscosity of ILs[24] and the need to image parallel to the IL/solid interface in plan-view. In this work, we report the direct observation of IL/oxide thin film interfaces, in cross-section, under bias using conventional and analytical transmission electron microscopy techniques. Specifically, the structural and chemical changes of IL/$La_{1/3}Sr_{2/3}FeO_3$ (LSFO) junctions are examined as a function of bias using high resolution imaging coupled with electron energy loss spectroscopy (EELS) in aberration-corrected scanning transmission electron microscopy (STEM). LSFO is a correlated oxide material that experiences a charge-ordering phase transition at 190 K and is of much research interest to those wishing to understand and control metal−insulator transitions in correlated oxides.[22,27] Specific to the material system investigated herein, we provide evidence that an irreversible chemical reaction occurs regardless of the applied bias, resulting in an intermixing region of 4−6 nm at the IL/oxide interface.

EXPERIMENTAL PROCEDURE

Materials and Film Growth. LSFO thin films were grown via molecular beam epitaxy on (001)-oriented $SrTiO_3$ substrates, followed by a postgrowth 200 °C anneal in a mixture of dilute ozone in oxygen at atmospheric pressure in order to minimize the concentration of oxygen vacancies in the film.[28] The IL used in this study, 1-ethyl-3-methylimidazolium hexafluorophosphate, obtained from Ionic Liquids Technologies, Inc., was chosen for its melting point of ∼60 °C, which ensures a solid state of the electrolyte at room temperature for the electron microscopy measurements. Note that this melting temperature is substantially higher than that of commonly used ILs in oxide gating experiments such as EMI-TFSI, DEME-BF_4, and DEME-TFSI.[29]

Electric-Double-Layer Formation. A 10 × 10 mm LSFO film was sectioned into four different samples: a control with no IL and no bias (0 V) and three samples with IL, 0, −1, and −2 V bias. These bias conditions were chosen to cover the representative range of applied voltages found in the literature.[10,12] All samples examined came from this single film growth to ensure consistency among the starting film conditions. The experiment proceeded as follows: a droplet of IL was heated to its melting temperature of approximately 60 °C and was placed on an unheated LSFO film. The film and IL were then heated above the IL melting temperature allowing for a gold wire electrode to be dipped into the IL and biased at the conditions previously outlined. The heat was then removed from the IL and film, while maintaining the bias, to allow the IL to solidify and freeze in the ionic arrangement.

Characterization. Electron transparent TEM samples were prepared via mechanical milling, followed by a conventional *in situ* lift-out procedure[30] using a FEI Strata DB 235 dual beam focused ion beam-scanning electron microscope. Bright field-TEM imaging was performed in a JEOL 2100 LaB_6 TEM operated at 200 kV. STEM imaging and EELS experiments were performed using an aberration corrected Nion UltraSTEM 100 operating at 100 kV,[31] which is equipped with a Gatan Enfina spectrometer. EEL spectra were processed with a power law background subtraction. EEL edge intensity maps were produced by integrating over a 40 eV window starting from the first peak of each edge reported. The peak positions from EELS, when reported, were obtained by fitting a Gaussian distribution to the spectra to find the peak maxima.

RESULTS AND DISCUSSION

High Resolution TEM Analysis. Conventional TEM analyses of the negatively biased IL/oxide films revealed different IL/oxide interfaces depending on the applied bias. High resolution BF-TEM images of the four LSFO samples (sectioned from the same film thus possessing the same initial composition and structure) are shown in Figure 1. Image analysis determined a LSFO film thickness of 18.5 ± 0.5 nm for the control, Figure 1a, 17 ± 1 nm for the 0 V sample, Figure 1b, 15 ± 2 nm for the −1 V bias sample, Figure 1c, and 17 ± 3 nm for the −2 V bias sample, Figure 1d. Our measured thickness values only consider the crystalline LSFO as the film. In a direct comparison to the control sample, the presence of IL alone degraded the LSFO film by 1.5 ± 1 nm. In addition, there was increased LSFO film roughness present between the control and 0 V samples, suggesting that the presence of this IL on LSFO resulted in an interfacial reaction. Furthermore, in both the −1 and −2 V samples, there was a clear electrochemical degradation of the LSFO thin film. A ∼2 nm thick secondary phase was present over approximately 70% of LSFO film surface in the −1 V sample. Lastly, the entire surface of the −2 V sample was degraded with over half of the LSFO film volume damaged below the original IL/film interface. In all samples analyzed, the oxide film appears to have been altered by the presence of IL.

Z-Contrast Imaging. High angle annular dark field STEM images (also known as Z-Contrast images)[32] of the 0 and −1 V films, shown in Figure 2, reveal an intermixing region at the IL/oxide interface. The most prominent feature of these images was the atomic number contrast found near the IL/LSFO interface. Neither the 0 V nor the −1 V samples contain an

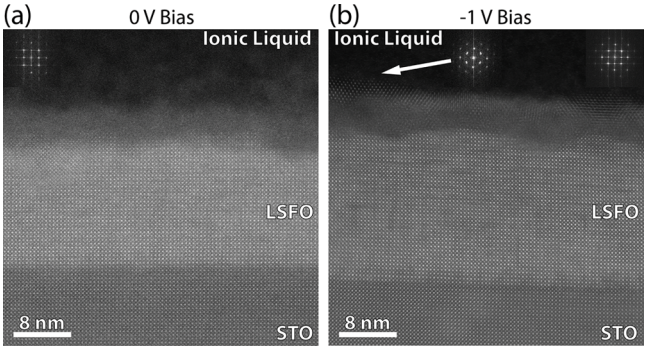

Figure 2. STEM-HAADF images with inset power spectra from the LSFO film: (a) 0 V sample. Note the 4−6 nm region of Z-Contrast above the LSFO film suggesting IL/LSFO intermixing at the interface. (b) −1 V sample showing a region of Z-Contrast above the LSFO film similar to (a) with a secondary polycrystalline phase on top of the film with inset power spectra from the secondary phase.

abrupt IL/LSFO interface; the STEM images suggest the IL/LSFO interface is within an intermixing region that has a thickness of 4−6 nm. In regions away from the interface, the LSFO film in the 0 V sample, Figure 2a, appeared to be unaffected by the IL, while the −1 V sample, Figure 2b, contained streaks of contrast that indicated the presence of aligned oxygen vacancies within the LSFO film.[33] Analysis of the fast Fourier transform (FFT) indicated that the phase found in the intermixing region of the −1 V sample indexed to a hexagonal structure consistent with the lattice spacing of (111)-oriented La_2O_3.[34]

Electron Energy Loss Spectroscopy. EELS analysis of both the 0 and −1 V samples revealed significant changes in the O K-, Fe L-, and La M-edges of both samples, which indicated intermixing of the IL and LSFO film in the interfacial region. A depth-resolved EELS edge intensity plot from the 0 V sample, shown in Figure 3a, indicated that both La and Fe were present within the IL several nm away from the film. The intermixing region between the IL and the LSFO was largely composed of La, which was the reason for the increased atomic number contrast observed in the HAADF images of the interfacial region. Furthermore, the composition of the LSFO film varied across the first 5 unit cells, decreasing in La content and increasing in Fe content, before it achieved consistency with the rest of the film.

Extracted core loss spectra chosen from specific areas of the IL/LSFO interface of the 0 V sample are shown in Figure 4a,b. The Fe $L_{3,2}$ near-edge fine structure, shown in Figure 4a, experiences a 1.1 ± 0.4 eV shift to higher energy upon crossing the IL/LSFO interface and moving into the LSFO film. The Fe L-edge in the IL and intermixing region exhibited a L_3 peak at 707.6 eV, which shifted to 708.7 eV five unit cells into the film; this is indicative of Fe valence being in a mixed $2^+/3^+$ state in the IL and intermixing region and in a mixed $3^+/4^+$ state within the LSFO film.[35] The Fe valence found within the LSFO film was consistent with past literature on the nominal valence of Fe in LSFO, which was reported to be nominally $Fe^{3.67+}$.[36,37] The O K-edge, shown in Figure 4b, consists of a single main peak in the IL and intermixing region, then develops a prepeak in the film, which indicates hybridization between O 2p and Fe 3d orbitals,[38] and after five unit cells into the film, the O K-edge splits into two separate peaks and remains this way throughout the rest of the film.

The depth-resolved edge intensity plot from the −1 V sample, shown in Figure 3b, exhibited strikingly different features compared to the 0 V sample. The EELS data indicates no significant concentration of La and Fe in the IL but revealed that the intermixing region consists of two compositionally different parts. The secondary phase, indexed previously to La_2O_3, consists predominantly of La, with minimal Fe, and a small amount of F from the IL. The incorporation of F, from the hexafluorophosphate anion, within the La_2O_3 layer strongly indicates electrochemical degradation. The area immediately below the secondary phase exhibits a high Fe and O concentration and slightly depleted La concentration. Below

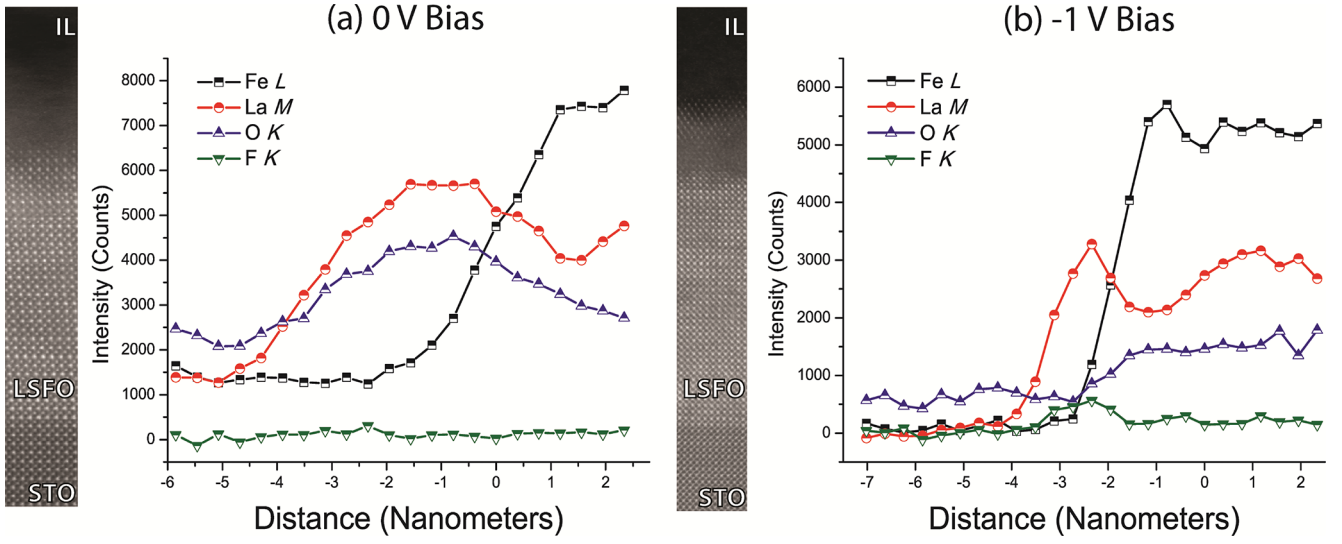

Figure 3. Integrated EELS edge intensity plots across the IL/LSFO interface with corresponding HAADF images. The *x*-axis indicates the LSFO film surface, with 0 indicating the surface, negative values moving into the IL and positive values moving into the LSFO film. (a) 0 V sample, note the presence of La and Fe in the IL and the high concentration of La in the intermixing region. The decrease in the O edge intensity within the LSFO film is due to the rise of a strong prepeak feature in the spectra. No F was observed in the 0 V sample. (b) −1 V sample, note the variance in composition of the intermixing region showing two compositionally distinct phases; the crystalline secondary phase exhibits a high La concentration as well as F from the IL. The integrated energy range for each spectrum is 40 eV starting from the first peak of each edge.

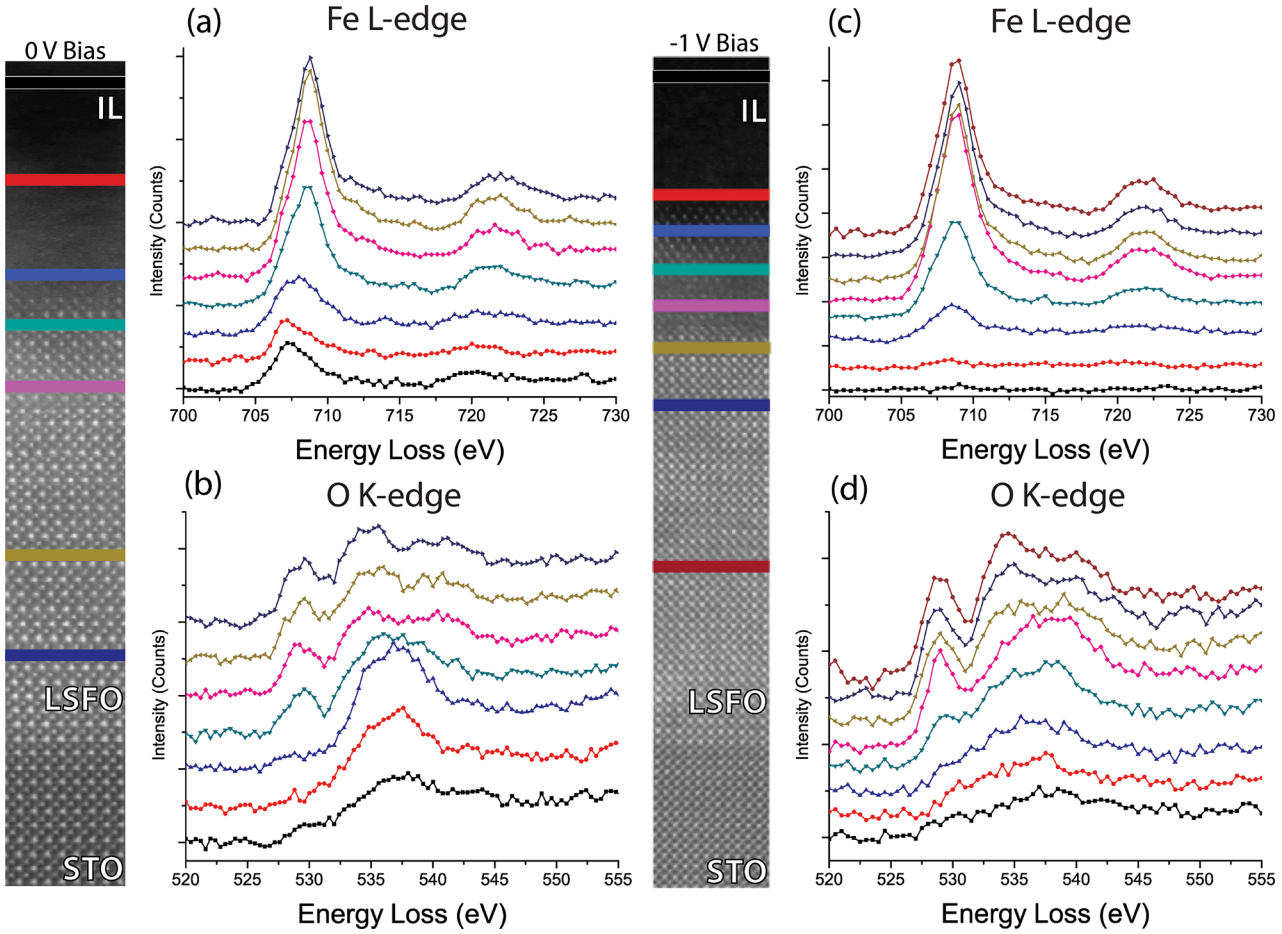

Figure 4. EELS fine structure of the Fe L- and O K-edge; all spectra have been processed with a power law background subtraction, and shown spectra are row averaged over 1 unit cell. (a) and (b) are the Fe L- and O K-edges of 0 V sample; the accompanying HAADF image with colored lines denotes the area where the spectra were taken. (c) and (d) are the Fe L- and O K-edges of the −1 V sample; the accompanying HAADF image denotes the area where the spectra were taken. The horizontal shift in the Fe L-edge in (a) is representative of a change in the oxidation state of Fe across the IL/LSFO interface through the first 5 unit cells of the film.

the Fe rich region, the film exhibits consistent edge intensities indicating little fluctuation in film composition outside of the first few unit cells.

Extracted core loss spectra chosen from specific areas of the IL/LSFO interface of the −1 V sample are shown in Figure 4c,d. The Fe $L_{3,2}$ near-edge structure, shown in Figure 4c, revealed no significant shift of the Fe L_3 edge across the entire intermixing region. The Fe L_3 peak was located at 708.8 eV and was similar to the one seen in the 0 V LSFO film, indicative of a mixed $3^+/4^+$ Fe valence state throughout the interfacial region and the LSFO film. The absence of any Fe valence shift suggested that there is no evidence for charge accumulation in this sample. The O K-edge, shown in Figure 4d, consisted of a single peak in the IL and then developed a prepeak feature at the bottom of the secondary phase, which increases linearly with Fe L_3 intensity throughout the intermixing region. The O K-edge spectra taken from the Fe and O rich area contains a well-defined prepeak and appears to be chemically shifted slightly to higher energies. The shape of the O K-edge is very similar to that observed from Fe_2O_3, suggesting that this region may consist of iron oxide.[35] When moving into the film, the O K-edge splits into two separate peaks after five unit cells and began to resemble the O K-edge of the 0 V sample.

CONCLUSIONS

The results from these measurements suggest two main points: (1) chemical intermixing occurred, over a 4−6 nm intermixing region, between the IL and LSFO thin film even in the absence of an applied bias and (2) the application of bias further degraded the LSFO thin film resulting in the formation of two compositionally different layers in the intermixing region. We rule out the possibility of FIB induced damage because the vacuum surface edge of the sample, which is normal to the ion beam during preparation and is prone to amorphization and ion-induced damage, is more than 100 nm away from all regions of analysis.[39] From Figure 1a,b, it is clear that IL reduced the LSFO film thickness by a few unit-cells compared with the IL-free control sample. The Z-Contrast images and EELS analysis confirmed the presence of La and Fe throughout the intermixing region of the 0 V sample. An applied bias of −1 V resulted in the formation of two compositionally different layers in the intermixing region, shown in Figure 3b. The most striking feature of the −1 V sample was the crystalline layer at the top of the intermixing region which structurally and chemically appears to be La_2O_3. The small amount of anion incorporation observed in the La_2O_3 further suggests electrochemical degradation. Although the electronic transport properties of these films were not measured, the formation of La_2O_3, an insulator with a high dielectric constant,[40] would

undoubtedly change the electrical properties of the IL/LSFO interface. The formation of this phase clearly indicates the presence of an electrochemical reaction, such as that seen during operation outside of the electrochemical stability window in this specific system.

While the transfer characteristics of an EDL-transistor system are subject to an electrochemical stability window, it is unclear whether that statement extends to the structure of the IL/oxide thin film interface present in the system. When directly compared with the previous studies mentioned employing $NdNiO_3$, $SrTiO_3$, and VO_2, they report no degradation due the chemical interaction between their IL and thin films at 0 V bias.[6,10,12,20,21,23] These results suggest that the IL observed here may be more reactive than ILs commonly used in field-effect experiments. It is important to note that, by heating the IL to 60 °C to perform our experiments, we may have an added thermal effect at the IL/LSFO interface; the possibility of this effect could be examined in future studies by varying the temperature of the IL droplet when it is placed on the oxide film. We caution against extrapolating our particular results to other systems. However, this experimental methodology can be used with other more common IL/oxide systems, taking advantage of cryo-based sample preparation and characterization techniques. We anticipate that the approach demonstrated herein can be applied to interfaces between ionic liquids and a wide variety of electronic materials, providing researchers with a powerful means to disentangle the complex physical and electrochemical interactions present at these heterojunctions. It is clear from our results that coupling high resolution and analytical TEM techniques with traditional EDL-transistor characterization will allow for a more accurate determination of safe operating parameters for IL-gated oxide device structures.

AUTHOR INFORMATION

Corresponding Author

*E-mail: mtaheri@coe.drexel.edu.

Notes

The authors declare no competing financial interest.

ACKNOWLEDGMENTS

This work was supported by Office of Naval Research, under grant numbers N00014-11-1-0664 and N00014-1101-0296, and through a user project supported by ORNL's Center for Nanophase Materials Sciences (CNMS), which is sponsored by the Scientific User Facilities Division, Office of Basic Energy Sciences, U.S. Department of Energy (JCI).

REFERENCES

(1) Ahn, C. H.; Triscone, J.-M.; Mannhart, J. Electric Field Effect in Correlated Oxide Systems. *Nature* **2003**, *424*, 1015−1018.

(2) Dawber, M.; Scott, J. F. Physics of Thin-Film Ferroelectric Oxides. *Rev. Mod. Phys.* **2005**, *77*, 1083−1130.

(3) Prabhumirashi, P.; Dravid, V. P.; Lupini, A. R.; Chisholm, M. F.; Pennycook, S. J. Atomic-Scale Manipulation of Potential Barriers at $SrTiO_3$ Grain Boundaries. *Appl. Phys. Lett.* **2005**, *87*, 121917.

(4) Takagi, H.; Hwang, H. Y. An Emergent Change of Phase for Electronics. *Science* **2010**, *327*, 1601−1602.

(5) Ahn, C. H.; Di Ventra, M.; Eckstein, J. N.; Frisbie, C. D.; Gershenson, M. E.; Goldman, A. M.; Inoue, I. H.; Mannhart, J.; Millis, A. J.; Morpurgo, A. F.; Natelson, D.; Triscone, J.-M. Electrostatic Modification of Novel Materials. *Rev. Mod. Phys.* **2006**, *78*, 1185−1212.

(6) Ueno, K.; Nakamura, S.; Shimotani, H.; Ohtomo, A.; Kimura, N.; Nojima, T.; Aoki, H.; Iwasa, Y.; Kawasaki, M. Electric-Field-Induced Superconductivity in an Insulator. *Nat. Mater.* **2008**, *7*, 855−858.

(7) Galiński, M.; Lewandowski, A.; Stępniak, I. Ionic Liquids as Electrolytes. *Electrochim. Acta* **2006**, *51*, 5567−5580.

(8) Misra, R.; McCarthy, M.; Hebard, A. F. Electric Field Gating with Ionic Liquids. *Appl. Phys. Lett.* **2007**, *90*, 052905.

(9) Ye, J. T.; Zhang, Y. J.; Akashi, R.; Bahramy, M. S.; Arita, R.; Iwasa, Y. Superconducting Dome in a Gate-Tuned Band Insulator. *Science* **2012**, *338*, 1193−1196.

(10) Ueno, K.; Shimotani, H.; Iwasa, Y.; Kawasaki, M. Electrostatic Charge Accumulation versus Electrochemical Doping in $SrTiO_3$ Electric Double Layer Transistors. *Appl. Phys. Lett.* **2010**, *96*, 252107.

(11) Ye, J. T.; Inoue, S.; Kobayashi, K.; Kasahara, Y.; Yuan, H. T.; Shimotani, H.; Iwasa, Y. Liquid-Gated Interface Superconductivity on an Atomically Flat Film. *Nat. Mater.* **2010**, *9*, 125−128.

(12) Asanuma, S.; Xiang, P.-H.; Yamada, H.; Sato, H.; Inoue, I. H.; Akoh, H.; Sawa, A.; Ueno, K.; Shimotani, H.; Yuan, H.; Kawasaki, M.; Iwasa, Y. Tuning of the Metal-Insulator Transition in Electrolyte-Gated NdNiO3 Thin Films. *Appl. Phys. Lett.* **2010**, *97*, 142110.

(13) Nakano, M.; Shibuya, K.; Okuyama, D.; Hatano, T.; Ono, S.; Kawasaki, M.; Iwasa, Y.; Tokura, Y. Collective Bulk Carrier Delocalization Driven by Electrostatic Surface Charge Accumulation. *Nature* **2012**, *487*, 459−462.

(14) Dhoot, A.; Israel, C.; Moya, X.; Mathur, N.; Friend, R. Large Electric Field Effect in Electrolyte-Gated Manganites. *Phys. Rev. Lett.* **2009**, *102*, 136402.

(15) Ji, H.; Wei, J.; Natelson, D. Modulation of the Electrical Properties of VO_2 Nanobeams Using an Ionic Liquid as a Gating Medium. *Nano Lett.* **2012**, *12*, 2988−2992.

(16) Lee, M.; Williams, J. R.; Zhang, S.; Frisbie, C. D.; Goldhaber-Gordon, D. Electrolyte Gate-Controlled Kondo Effect in $SrTiO_3$. *Phys. Rev. Lett.* **2011**, *107*, 256601.

(17) Lee, Y.; Clement, C.; Hellerstedt, J.; Kinney, J.; Kinnischtzke, L.; Leng, X.; Snyder, S. D.; Goldman, A. M. Phase Diagram of Electrostatically Doped $SrTiO_3$. *Phys. Rev. Lett.* **2011**, *106*, 136809.

(18) Scherwitzl, R.; Zubko, P.; Lezama, I. G.; Ono, S.; Morpurgo, A. F.; Catalan, G.; Triscone, J.-M. Electric-Field Control of the Metal-Insulator Transition in Ultrathin $NdNiO_3$ Films. *Adv. Mater.* **2010**, *22*, 5517−5520.

(19) Liu, K.; Fu, D.; Cao, J.; Suh, J.; Wang, K. X.; Cheng, C.; Ogletree, D. F.; Guo, H.; Sengupta, S.; Khan, A.; Yeung, C. W.; Salahuddin, S.; Deshmukh, M. M.; Wu, J. Dense Electron System from Gate-Controlled Surface Metal-Insulator Transition. *Nano Lett.* **2012**, *12*, 6272−6277.

(20) Li, M.; Han, W.; Jiang, X.; Jeong, J.; Samant, M. G.; Parkin, S. S. P. Suppression of Ionic Liquid Gate-Induced Metallization of $SrTiO_3$(001) by Oxygen. *Nano Lett.* **2013**, *13*, 4675−4678.

(21) Jeong, J.; Aetukuri, N.; Graf, T.; Schladt, T. D.; Samant, M. G.; Parkin, S. S. P. Suppression of Metal-Insulator Transition in VO_2 by Electric Field-Induced Oxygen Vacancy Formation. *Science* **2013**, *339*, 1402−1405.

(22) Ma, J.; Yan, J.-Q.; Diallo, S. O.; Stevens, R.; Llobet, A.; Trouw, F.; Abernathy, D. L.; Stone, M. B.; McQueeney, R. J. Role of Magnetic Exchange Energy on Charge Ordering in $R_{1/3}Sr_{2/3}FeO_3$ (R = La, Pr, and Nd). *Phys. Rev. B* **2011**, *84*, 224115.

(23) Zhou, Y.; Ramanathan, S. Relaxation Dynamics of Ionic Liquid—VO_2 Interfaces and Influence in Electric Double-Layer Transistors. *J. Appl. Phys.* **2012**, *111*, 084508.

(24) Yokota, Y.; Harada, T.; Fukui, K. Direct Observation of Layered Structures at Ionic Liquid/Solid Interfaces by Using Frequency-Modulation Atomic Force Microscopy. *Chem. Commun.* **2010**, *46*, 8627−8629.

(25) Negami, M.; Ichii, T.; Murase, K.; Sugimura, H. Visualization of Ionic-Liquid/Solid Interfaces by Frequency Modulation Atomic Force Microscopy. *ECS Trans.* **2013**, *50*, 349−355.

(26) Segura, J. J.; Elbourne, A.; Wanless, E. J.; Warr, G. G.; Voïtchovsky, K.; Atkin, R. Adsorbed and Near Surface Structure of

Ionic Liquids at a Solid Interface. *Phys. Chem. Chem. Phys.* **2013**, *15*, 3320−3328.
(27) Park, S. K.; Ishikawa, T.; Tokura, Y.; Li, J. Q.; Matsui, Y. Variation of Charge-Ordering Transitions in $R_{1/3}Sr_{2/3}FeO_3$ (R = La, Pr, Nd, Sm, and Gd). *Phys. Rev. B* **1999**, *60*, 788−795.
(28) Xie, Y.; Scafetta, M. D.; Sichel-Tissot, R. J.; Moon, E. J.; Devlin, R. C.; Wu, H.; Krick, A. L.; May, S. J. Control of Functional Responses Via Reversible Oxygen Loss in $La_{1-X}Sr_XFeO_{3-\Delta}$ Films. *Adv. Mater.* **2014**, *26*, 1434−1438.
(29) Zhou, Y.; Ramanathan, S. Correlated Electron Materials and Field Effect Transistors for Logic: A Review. *Crit. Rev. Solid State Mater. Sci.* **2013**, *38*, 286−317.
(30) Langford, R. M.; Rogers, M. In Situ Lift-out: Steps to Improve Yield and a Comparison with Other FIB TEM Sample Preparation Techniques. *Micron* **2008**, *39*, 1325−1330.
(31) Krivanek, O. L.; Corbin, G. J.; Dellby, N.; Elston, B. F.; Keyse, R. J.; Murfitt, M. F.; Own, C. S.; Szilagyi, Z. S.; Woodruff, J. W. An Electron Microscope for the Aberration-Corrected Era. *Ultramicroscopy* **2008**, *108*, 179−195.
(32) Browning, N. D.; Chisholm, M. F.; Pennycook, S. J. Atomic-Resolution Chemical Analysis Using a Scanning Transmission Electron Microscope. *Nature* **1993**, *366*, 143−146.
(33) Klie, R. F. Characterization of Oxygen Ordering in (La, Sr)$FeO_{3-\delta}$ by Atomic Resolution Z-Contrast Imaging and Electron Energy-Loss Spectroscopy. *J. Electron Microsc. (Tokyo)* **2002**, *51*, 59S−66.
(34) Wang, C.; Tan, M.; Feng, C.; Ma, Z.; Jiang, S.; Xu, Z.; Cao, G.; Matsubayashi, K.; Uwatoko, Y. $La_2Co_2Se_2O_3$: A Quasi-Two-Dimensional Mott Insulator with Unusual Cobalt Spin State and Possible Orbital Ordering. *J. Am. Chem. Soc.* **2010**, *132*, 7069−7073.
(35) Tan, H.; Verbeeck, J.; Abakumov, A.; Van Tendeloo, G. Oxidation State and Chemical Shift Investigation in Transition Metal Oxides by EELS. *Ultramicroscopy* **2012**, *116*, 24−33.
(36) Takano, M.; Kawachi, J.; Nakanishi, N.; Takeda, Y. Valence State of the Fe Ions in $Sr_{1-y}La_yFeO_3$. *J. Solid State Chem.* **1981**, *39*, 75−84.
(37) Battle, P. D.; Gibb, T. C.; Lightfoot, P. The Structural Consequences of Charge Disproportionation in Mixed-Valence Iron Oxides. I. The Crystal Structure of $Sr_2LaFe_3O_{8.94}$ at Room Temperature and 50 K. *J. Solid State Chem.* **1990**, *84*, 271−279.
(38) De Groot, F.; Grioni, M.; Fuggle, J.; Ghijsen, J.; Sawatzky, G.; Petersen, H. Oxygen 1s X-Ray-Absorption Edges of Transition-Metal Oxides. *Phys. Rev. B* **1989**, *40*, 5715−5723.
(39) Giannuzzi, L. A.; Geurts, R.; Ringnalda, J. 2 keV Ga+ FIB Milling for Reducing Amorphous Damage in Silicon. *Microsc. Microanal.* **2005**, *11*, 828−829.
(40) Robertson, J. Interfaces and Defects of High-K Oxides on Silicon. *Solid-State Electron.* **2005**, *49*, 283−293.